The FEBS Journal

FEBS PRESS science publishing by scientists

The small molecule ZPD-2 inhibits the aggregation and seeded polymerisation of C-terminally truncated α-Synuclein

Samuel Peña-Díaz[1,2,*] and Salvador Ventura[1,2,3]

1 Institut de Biotecnologia i Biomedicina, Universitat Autònoma de Barcelona, Bellaterra, Spain
2 Departament de Bioquímica i Biologia Molecular, Universitat Autònoma de Barcelona, Bellaterra, Spain
3 Hospital Universitari Parc Taulí, Institut d'Investigació i Innovació Parc Taulí (I3PT-CERCA), Universitat Autònoma de Barcelona, Sabadell, Spain

Keywords
inhibition; oligomer; protein aggregation; truncation; α-Synuclein

Correspondence
S. Peña-Díaz, Interdisciplinary Nanoscience Center (iNANO), 1592-228, Aarhus University (AU), Gustav Wieds Vej 14, DK-8000 Aarhus C, Denmark
Tel: +45 8715 0000
E-mail: samuelpd@inano.au.dk
and
S. Ventura, Instituto de Biotecnología y de Biomedicina, Universitat Autònoma de Barcelona, Edifici MRB. Carrer de la Vinya, s/n. Campus, 08193 Cerdanyola del Vallès, Barcelona, Spain
Tel: +34 93 586 8956
E-mail: salvador.ventura@uab.cat

Present address
Department of Molecular Biology and Genetics, Interdisciplinary Nanoscience Centre (iNANO), Aarhus University, Aarhus, Denmark

(Received 11 July 2024, revised 26 August 2024, accepted 16 October 2024)

doi:10.1111/febs.17310

Protein aggregation, particularly the formation of amyloid fibrils, is associated with numerous human disorders, including Parkinson's disease. This neurodegenerative condition is characterised by the accumulation of α-Synuclein amyloid fibrils within intraneuronal deposits known as Lewy bodies or neurites. C-terminally truncated forms of α-Synuclein are frequently observed in these inclusions in the brains of patients, and their increased aggregation propensity suggests a role in the disease's pathogenesis. This study demonstrates that the small molecule ZPD-2 acts as a potent inhibitor of both the spontaneous and seeded amyloid polimerisation of C-terminally truncated α-Synuclein by interfering with early aggregation intermediates. This dual activity positions this molecule as a promising candidate for therapeutic development in treating synucleinopathies.

Introduction

Parkinson's disease (PD) is the second most prevalent neurodegenerative disorder worldwide, after Alzheimer's disease [1,2]. Its defining feature is the loss of dopamine-producing neurons in the *substantia nigra pars compacta*, leading to characteristic motor symptoms such as tremor, rigidity and/or bradykinesia [3,4].

Abbreviations
ATR-FTIR, attenuated total reflection Fourier-transform infrared; NAC, non-Amyloid Corecore; PD, Parkinson's disease; PQQ, pyrroloquinoline quinone; SC-D, SynuClean-D; TEM, transmission electron microscopy; Th-T, Thioflavin-T; α-Syn, α-Synuclein; α-Syn-CT, C-terminal truncated α-Syn; α-Syn-FL, full-length α-Syn.

However, PD may also involve non-motor complications such as dementia [5,6].

Like other neurodegenerative pathologies, PD is connected with the presence of amyloid protein deposits in the brain [7]. The major histopathological hallmark of PD is the formation of intraneuronal aggregates in neuronal bodies and processes, named Lewy bodies and neurites. These assemblies are primarily composed of amyloid fibrils formed by the protein α-Synuclein (α-Syn) [7]. Under normal conditions, α-Syn exists as a soluble and mostly disordered protein that participates in diverse functions, including regulating vesicle trafficking, fatty acid binding and neuronal survival [8–13], whereas in pathological conditions, the protein misfolds and establishes intermolecular β-sheet interactions to form toxic and neuron-to-neuron transmissible aggregates [14].

The 140-residue amino acid sequence of α-Syn can be dissected into three distinct regions: N-terminal, non-amyloid core (NAC) domain and C-terminal [15]. The hydrophobic NAC domain drives the formation of cross-β amyloid aggregates, whereas the N- and C-terminal regions appear to modulate this process [16–18]. The N-terminal is highly conserved and contains most of the imperfect KTKEGV repeats responsible for the amphipathic character of α-Syn and its interactions with lipids, which are important for both its functional and pathogenic behaviour [19,20]. The C-terminal region has been described to act as an intramolecular chaperone that reduces the aggregation propensity of the full-length protein [21,22]. This α-Syn segment is highly flexible and has many acidic residues (10 glutamates + 5 aspartates), providing a high negative charge that precludes or delays amyloid formation through repulsive electrostatic interactions [22,23]. In this way, truncation of the α-Syn C-terminus significantly increases its aggregation, supporting a solubilising role for this domain [24–26].

Truncated forms of α-Syn are detected in healthy brains, but there is an enrichment of C-terminal truncated α-Syn (α-Syn-CT) in the protein deposits of PD patients [27]. C-terminal truncations are thought to result from an incomplete degradation in the proteasome [28,29] and the activity of endoproteases such as calpain [29,30], with cellular and *in vivo* studies showing that truncation precedes and increases fibrillation [31]. The enhancement of α-Syn aggregation propensity is proportional to the extent of the truncation, as long as it does not affect the NAC domain (residues 85–90) [32]. C-terminal truncation enhances mitochondrial degradation, leading to an increased toxicity [33], and transgenic mice expressing C-terminal truncated species manifest PD-like symptoms [34]. Furthermore, it has been shown that the aggregation of α-Syn-CT induces the pathological accumulation of the full-length protein [25,34–36].

The exacerbated aggregation propensity of α-Syn-CT likely underlies the limited success in identifying small molecules that effectively inhibit its amyloidogenesis. While there have been numerous reports on small organic molecules modulating the aggregation of the full-length α-Syn (α-Syn-FL) [37–39], to our knowledge, only one compound, pyrroloquinoline quinone (PQQ) (Fig. 1), has been reported to be effective against the truncated variant [40]. In this study, we explored the impact of two small molecules, SynuClean-D (SC-D) and ZPD-2 (Fig. 1), on the polymerisation of one of the most common C-terminal truncations, the isoform containing residues 1–119 (α-Syn-CT119) [28,29]. Both compounds have recently

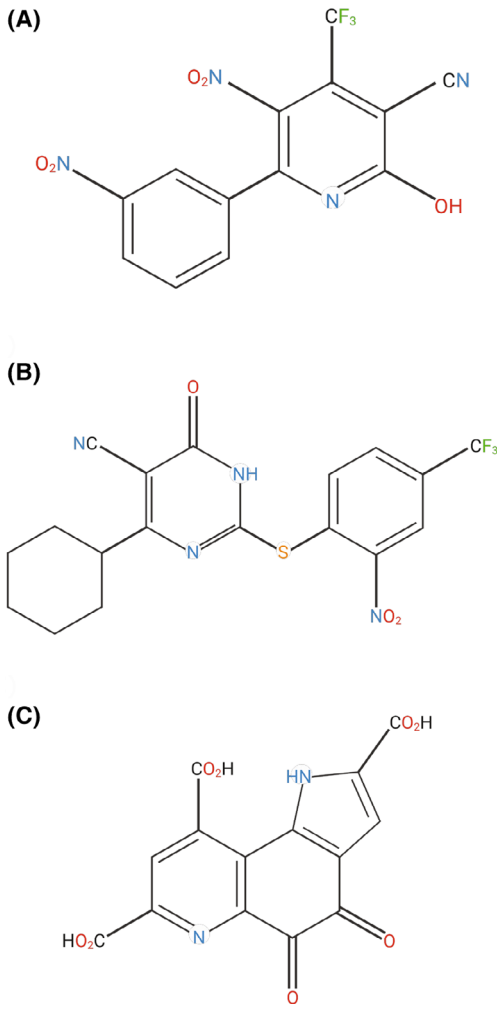

Fig. 1. Modulators of α-Syn-CT119 aggregation. (A–C) Chemical structure of SynuClean-D (A), ZPD-2 (B) and PQQ (C).

been described as potent modulators of α-Syn-FL aggregation both *in vitro* and in *C. elegans* models of PD, exerting a neuroprotective effect on dopaminergic neurons [41,42]. Consistent with previous findings [25,43], this truncated variant exhibited a significantly higher aggregation propensity when compared to α-Syn-FL. However, ZPD-2 was highly effective in inhibiting both the spontaneous and seeded polymerisation of α-Syn-CT119 by targeting preferentially the truncated oligomeric species. Therefore, this molecule is a dual agent able to interfere with the aggregation of intact and truncated α-Syn, holding potential for therapeutic development.

Results

Impact of α-syn C-terminal truncation on its aggregation

The presence of naturally occurring truncated variants in the brains of PD patients suggests a potential role for truncation in disease progression. Several truncations have been described *in vivo* (103, 110, 113, 114, 115, 119, 122, 124, 125, 133, and 135), but truncations at positions 119 and 122 are most prevalent, with levels as high as 20–25% that of α-Syn-FL in the insoluble brain fraction [28,29]. We compared the aggregation propensity of the α-Syn-CT119 isoform with that of α-Syn-FL using a kinetic assay that monitors the characteristic increase in fluorescence intensity of Thioflavin-T (Th-T) upon binding to amyloid fibrils. The level of fluorescence attained by α-Syn-CT119 at the end of the polymerisation reaction was 2.3-fold greater than that of α-Syn-FL (Fig. 2A), consistent with previous studies [43]. In addition, truncation dramatically accelerated the rate of fibril formation (Fig. 2A), shortening the lag phase by 6.7 h (from 11.2 to 4.5 h) due to a 90-fold increase in the primary nucleation rate ($K_b = 0.03843$ vs $K_b = 0.00043$). This acceleration notably shortened the T_{50} of the reaction by 6.8 h (from 11.3 to 4.5).

Transmission electron microscopy (TEM) analysis revealed differences in α-Syn-FL and α-Syn-CT119 fibrils morphology (Fig. 2D,E). α-Syn-FL tends to form large and well-defined ribbon-like fibrils (Fig. 2E), whereas α-Syn-CT119 fibrils are clearly shorter and have a rod-like shape. To date, all high-resolution structures of α-Syn-FL fibrils have consistently shown that the flexible C-terminal region remains unincorporated within the amyloid core [14,17,18,44–46]. This configuration results in a surrounding cloud of negative charge enveloping the fibril surface, thereby impeding lateral association. Truncated fibrils lack this flexible anionic region, which translates into the formation of larger, denser and more frequent aggregate clusters compared to α-Syn-FL (Fig. 3).

We investigated whether the observed differences in fibril morphology and stickiness correlate with differences in the secondary structure content using attenuated total reflection Fourier-transform infrared (ATR-FTIR) spectroscopy. Specifically, we recorded the infrared signal in the amide I region of the spectrum (1700–1600 cm^{-1}) (Fig. 2B,C and Table 1). In α-Syn-CT119 fibrils, the spectrum was dominated by a signal at 1628 cm^{-1}, assigned to intermolecular β-sheets, accounting for 52% of the area, whereas the unordered signal at 1648 cm^{-1} contributed only 7%. In contrast, in α-Syn-FL fibrils, the intermolecular β-sheets and unordered signals account for 36% and 32% of the spectrum area, respectively. These data suggest that α-Syn-CT119 and α-Syn-FL fibrils share similar core regions, albeit not necessarily in the same spatial configuration, but α-Syn-CT119 is devoid of the disordered regions that surround and exclude lateral interactions in full-length fibrils.

Impact of SynuClean-D and ZPD-2 on α-syn-CT119 aggregation kinetics

SC-D and ZPD-2 were previously shown to be potent modulators of α-Syn-FL aggregation, both *in vitro* and *in vivo* [41,42,47]. We assayed here whether they are also able to inhibit the aggravated aggregation observed in α-Syn-CT119. Incubation of 35 μM of α-Syn-CT119 in the presence of 50 μM of SC-D revealed that the molecule inhibited the protein aggregation, reducing the formation of Th-T positive species at the end of the reaction by 51.5% (Fig. 4A), although it seemed to be less effective than against the aggregation of α-Syn-FL, where Th-T fluorescence was reduced by 71.5% (Fig. 4C). At the same concentration, ZPD-2 was exceptionally active, abrogating almost completely the formation of fibrils, with a 96.9% reduction in Th-T fluorescence emission (Fig. 4A), being similarly active against α-Syn-FL aggregation, with a 97.3% reduction (Fig. 4C).

Validation and characterisation of the inhibitory activity of the compounds

Orthogonal light-scattering measurements at the end-point of the aggregation reaction confirmed that the observed reduction in Th-T fluorescence correlates with a significant decrease in the levels of detectable α-Syn-CT119 and α-Syn-FL aggregates, with reductions

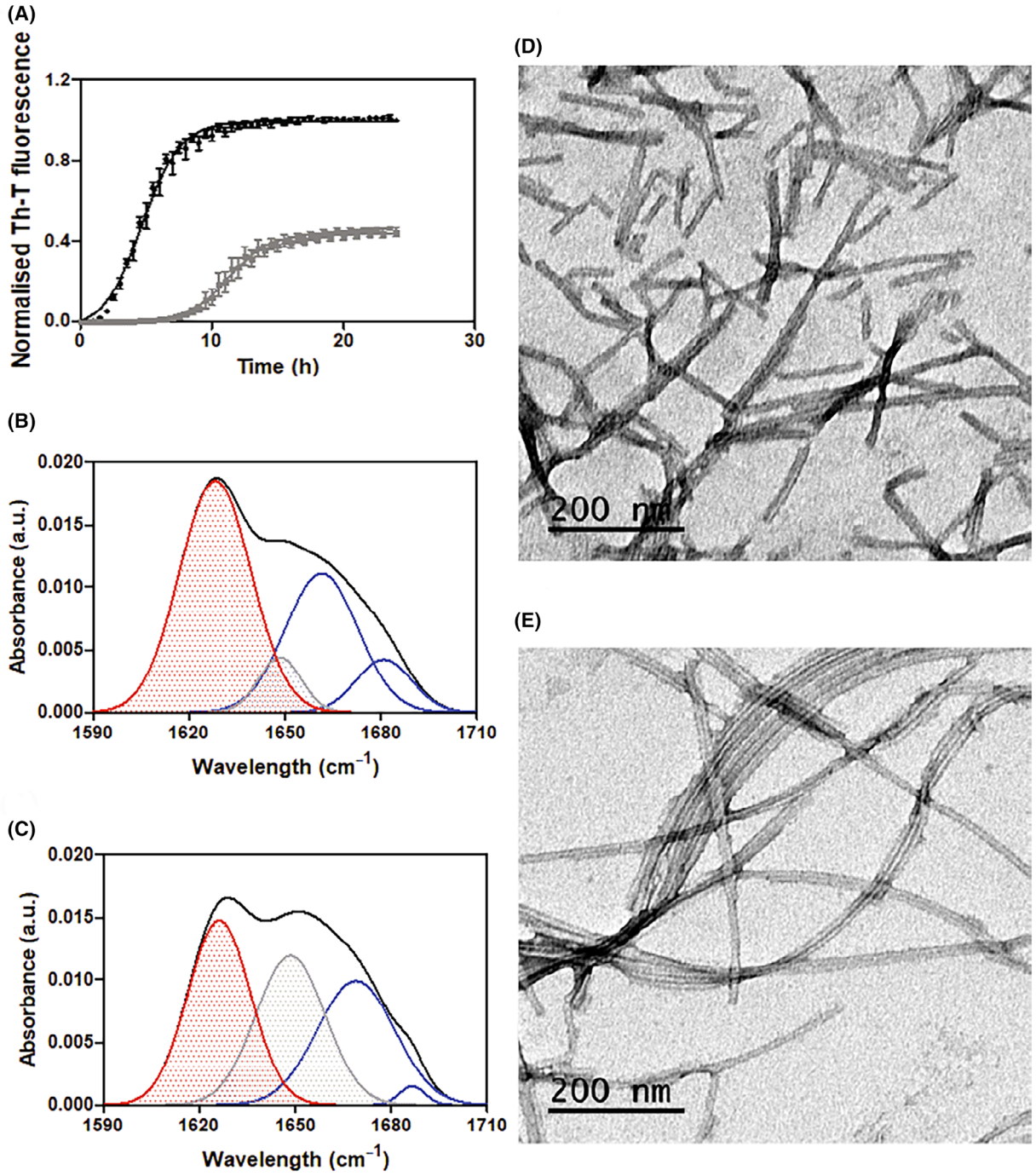

Fig. 2. Characterisation of C-terminally truncated α-Synuclein aggregation. (A) Kinetic analysis of C-terminally truncated (black) and *wt* (grey) α-Syn aggregation followed by Th-T fluorescence measurement. Th-T fluorescence is plotted as normalised means. Error bars are shown as standard errors of mean values. (B, C) Secondary structure characterisation reported by ATR-FTIR absorbance spectra in the amide I region of final point aggregates of truncated (B) and *wt* (C) mature fibrils. (D, E) Representative TEM images of C-terminally truncated (D) and *wt* (E) α-Syn fibrils. Scale bar 200 nm. All the experimental data, acquired in three independent experiments ($n = 3$).

in dispersed light of 31.7% and 53.03% for SC-D and ZPD-2, respectively (Fig. 4B,D). TEM images further corroborated that the samples treated with SC-D, and especially those treated with ZPD-2, exhibited significantly fewer α-Syn-CT119 fibrils per field and displayed less clustering than untreated ones (Fig. 4E–G).

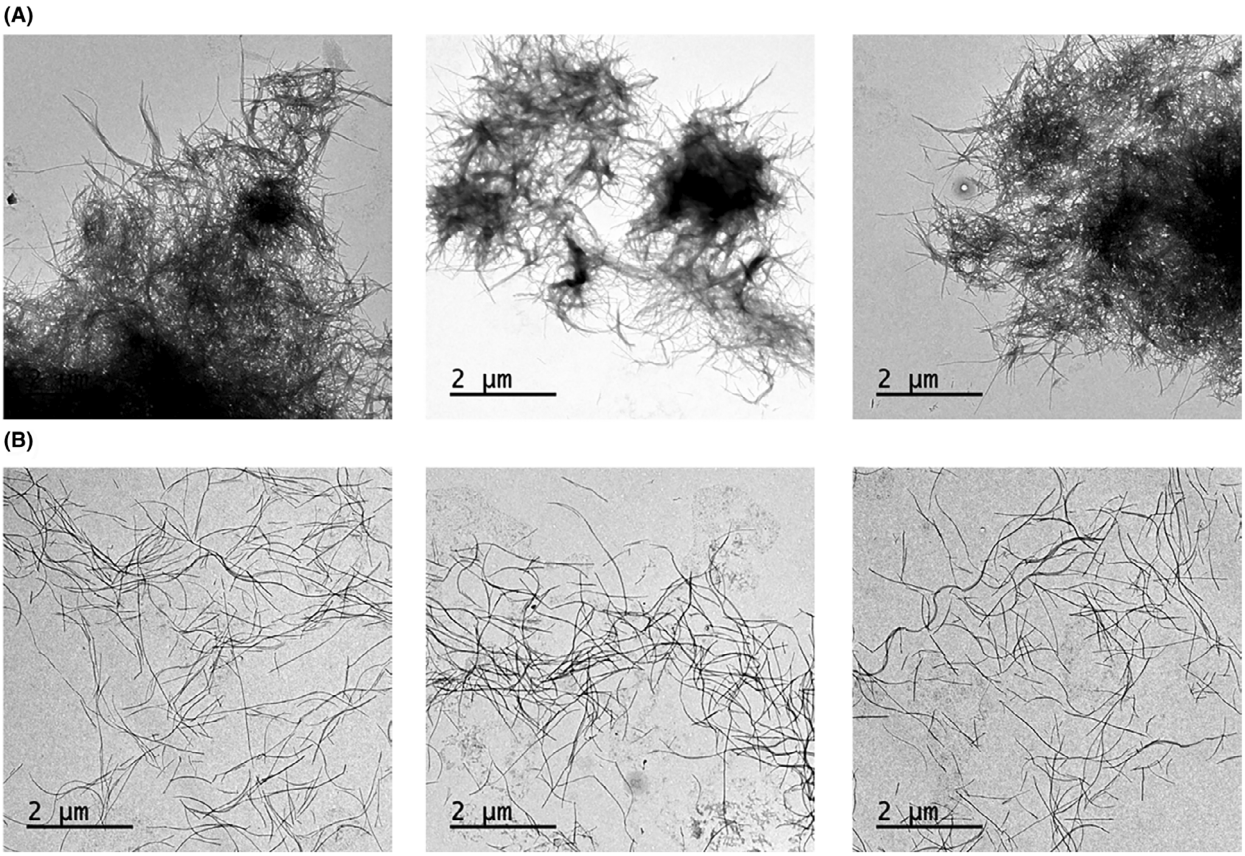

Fig. 3. Low magnification TEM images of α-Synuclein mature fibrils. Representative TEM images at 1500× of C-terminally truncated (A) and *wt* (B) mature α-Syn fibrils. Scale bar 2 μm. All the experimental data, acquired in three independent experiments ($n = 3$).

Table 1. Assignment of the fibrils secondary structure. The secondary structure content of C-terminally truncated and wt α-Syn aggregates at the reaction final point were obtained by measuring ATR-FTIR absorbance in the amide I region of the spectra. The fitted individual bands after Gaussian deconvolution are indicated.

Truncated			WT		
Band (cm^{-1})	Area (%)	Structure	Band (cm^{-1})	Area (%)	Structure
1628	52	β-sheet (inter)	1626	36	β-sheet (inter)
1648	7	Unordered	1648	32	Unordered
1661	31	β-turn	1669	30	β-turn
1681	9	β-turn	1687	1	β-turn

Subsequently, we performed a titration analysis to assess whether the inhibitory activity of these molecules was dose-dependent (Fig. 5A,B), as previously reported for α-Syn-FL [41,42]. This assay revealed that ZPD-2 was notably more potent than SC-D against α-Syn-CT119 aggregation, with ZPD-2 showing significant activity at 25 and 10 μM, corresponding to 1.4:1 and 3.5:1 protein-to-molecule ratios, where it promoted 69.36% and 39.42% reduction in Th-T fluorescence, respectively. SC-D displayed low or no activity at the same concentrations, which contrasts with our previous observations for α-Syn-FL [42]. Thus, ZPD-2 is active at substoichiometric concentrations, displaying significantly greater inhibitory activity against α-Syn-CT119 aggregation than the one previously reported for PQQ (Fig. 5C).

To determine the time window during which the two molecules are active, we set up aggregation reactions of α-Syn-CT119 in which 50 μM of the molecules were added at 0 h, 2.5 h and 5 h after the reaction commenced. At 2.5 h and 5 h, the exponential phase of the aggregation reaction has progressed by 11.48% and 61.75%, respectively. While SC-D turned out to be insensitive to the time of addition, the activity of ZPD-2 was clearly time-dependent, exhibiting its strong inhibitory effect only when added at the beginning of the aggregation (Fig. 6A,B). This suggests that ZPD-2 is primarily active against the species formed early in the fibrillation reaction. A similar dependence

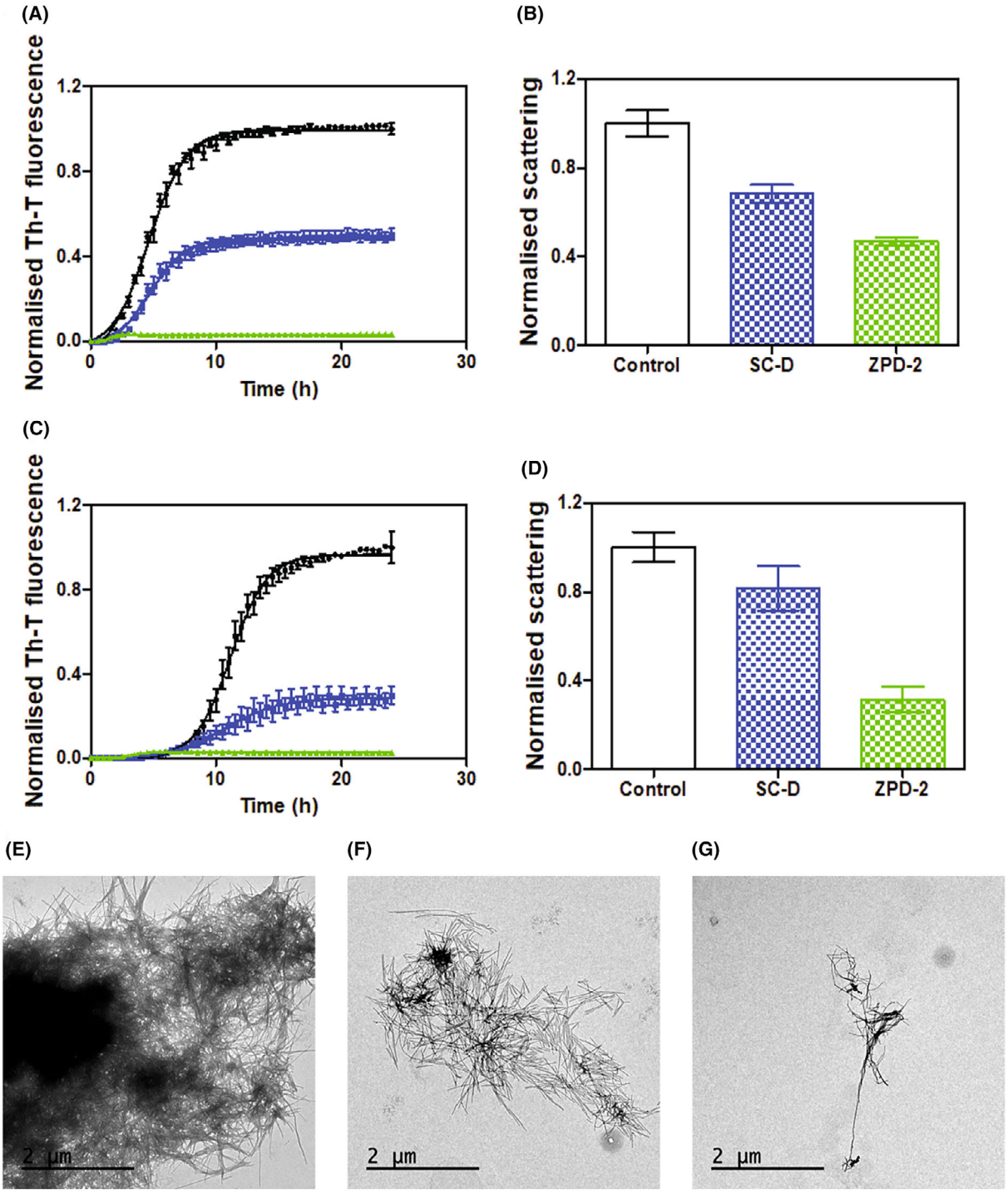

Fig. 4. Inhibition of C-terminally truncated and full-length α-Synuclein aggregation. (A) Aggregation of C-terminally truncated α-Syn in absence (black) or presence of SC-D (blue) and ZPD-2 (green). The aggregation is followed by Th-T fluorescence measurement. (B) Final point light-scattering measurements of truncated mature α-Syn fibrils formed in absence (black) or presence of SC-D (blue) and ZPD-2 (green). (C) Aggregation of full-length α-Syn in absence (black) or presence of SC-D (blue) and ZPD-2 (green). The aggregation is followed by Th-T fluorescence measurement. (D) Final point light-scattering measurements of mature α-Syn fibrils formed in absence (black) or presence of SC-D (blue) and ZPD-2 (green). Th-T fluorescence and light scattering are plotted as normalised means. Error bars are shown as standard errors of mean values. (E–G) Representative TEM images of mature fibrils of C-terminally truncated α-Syn in absence (E) or presence of SC-D (F) and ZPD-2 (G). Scale bar 2 µm. All the experimental data, acquired in three independent experiments ($n = 3$).

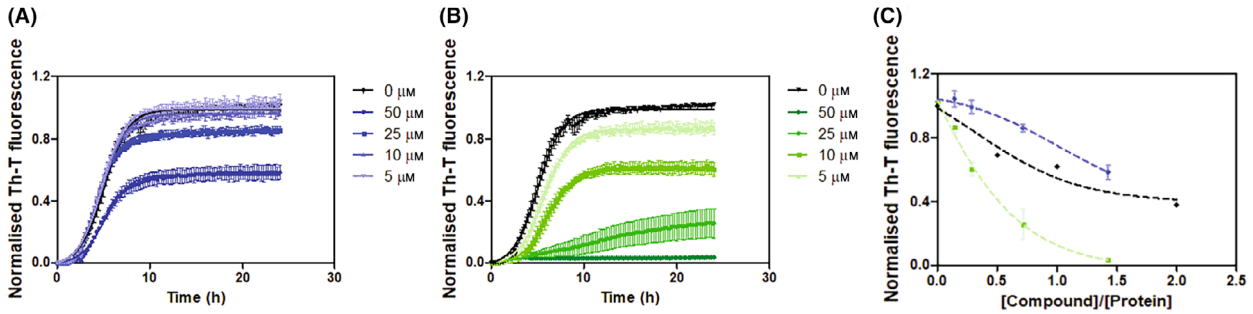

Fig. 5. Concentration-dependent activity. (A–C) Aggregation of C-terminally truncated α-Syn in absence (black) or presence of different concentrations (0, 5, 10, 25 and 50 μM) of SC-D (A) and ZPD-2 (B). The aggregation is followed by Th-T fluorescence measurement. Th-T fluorescence is plotted as normalised means. Error bars are shown as standard errors of mean values. (C) Concentration-dependent activity of PQQ (black), SC-D (blue) and ZPD-2 (green). PQQ values are derived from literature [40]. All the experimental data, acquired in three independent experiments ($n = 3$).

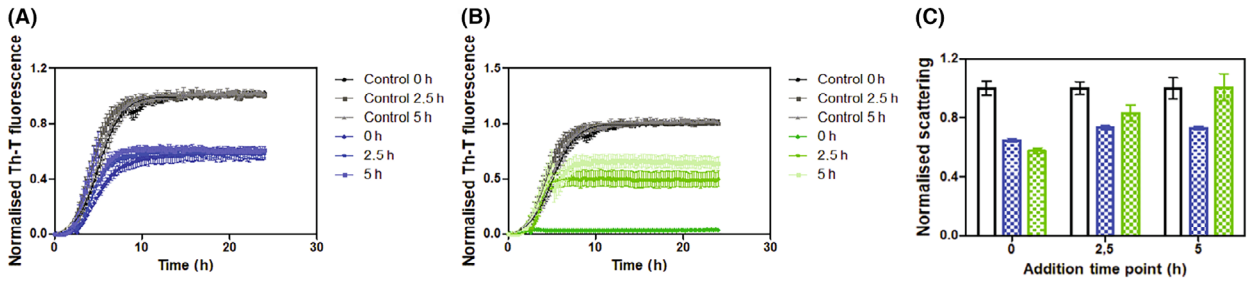

Fig. 6. Time-dependent activity. (A, B) Aggregation of C-terminally truncated α-Syn in absence (black) or presence of 50 μM of SC-D (A) and ZPD-2 (B) added at different time points of the reactions. The aggregation is followed by Th-T fluorescence measurement. (C) Final point light-scattering measurements of mature α-Syn fibrils formed in absence (black) or presence of 50 μM of SC-D (blue) and ZPD-2 (green). Th-T fluorescence and light-scattering are plotted as normalised means. Error bars are shown as standard errors of mean values. All the experimental data, acquired in three independent experiments ($n = 3$).

of the signal on the time of ZPD-2 addition was observed when measuring orthogonal light scattering at the endpoint of the reaction (Fig. 6C).

Modulation of α-syn-CT119 oligomers

We have shown previously that neither SC-D nor ZPD-2 binds to isotopically labelled monomeric and soluble α-Syn-FL [41,42]. Due to the high aggregation propensity of α-Syn-CT119, we were unable to repeat these experiments with the truncated variant. However, given that the sequence of α-Syn-CT119 is encompassed within the full-length protein, we do not anticipate specific interactions of ZPD-2 and the initially soluble state α-Syn-CT119. This led us to consider that the target of this molecule may be the early oligomeric species.

Truncated forms of α-Syn have been shown to form prefibrillar, oligomeric structures [48]. Nonetheless, because of the lack of the solubilising C-terminal region, truncated oligomers exhibit higher exposed hydrophobicity and can laterally interact, becoming significantly resistant to chaperone-mediated disaggregation [48]. By implementing the same protocol previously used to obtain α-Syn-FL oligomers [49], we successfully obtained highly homogenous preparations of α-Syn-CT119 oligomers (Fig. 7D).

We assessed the impact of SC-D and ZPD-2 on truncated α-Syn oligomers using TEM. After incubating oligomers with SC-D for 24 h, little change in particle organisation and number was observed (Fig. 7A–C,E). Conversely, treatment with ZPD-2 dramatically reduced the number of observable oligomers. Furthermore, the remaining assemblies were less spheric and tended to cluster together (Fig. 7A–C,F). These data indicate that ZPD-2 interacts with and disentangles structured α-Syn-CT119 oligomers, potentially by modifying their surface properties.

Impact of SynuClean-D and ZPD-2 on α-syn-CT119 seeded polymerisation

The formation of amyloid fibrils can be accelerated or induced by the addition of previously formed aggregates [50]. This process, usually referred to as seeding,

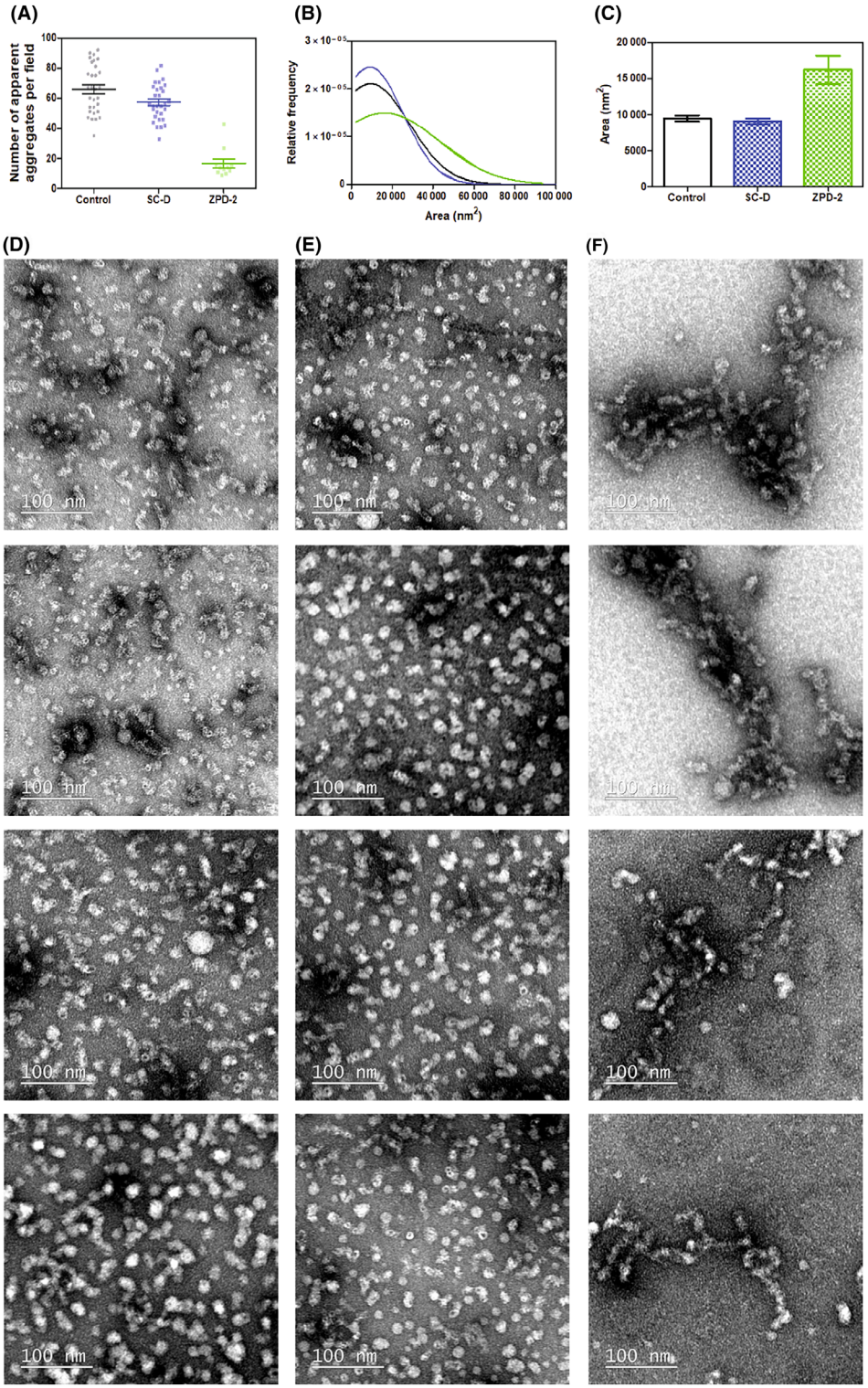

Fig. 7. Effect of the compounds on the C-terminally truncated oligomers. (A) Quantification of the number of particles observed on TEM images. (B) Area distribution of the observed structures in absence (black) or presence of 100 μM of SC-D (blue) or ZPD-2 (green). (C) Mean areas of the different samples according to TEM images. Error bars are shown as standard errors of mean values. (D–F) Representative TEM images of the oligomers treated for 20 h with DMSO (D), SC-D (E) or ZPD-2 (F). All the experimental data, acquired in three independent experiments ($n = 3$).

plays a key role in the pathogenesis and spreading of the disease, as preformed aggregates can propagate to neighbouring cells in a prion-like manner [51–54]. Accordingly, evaluating the capacity of a molecule to prevent these events is crucial for it to become an effective anti-aggregational therapy.

The addition of 0.1% (v/v) of preformed and sonicated α-Syn-FL fibrils to its soluble counterpart effectively accelerated amyloid formation by shortening the lag phase, consistent with previous reports [25,34–36] (Fig. 8). This effect was observable, but much less pronounced for α-Syn-CT119, which displays an extremely short lag phase even without seeds (Fig. 8A). Additionally, we also explored cross-seeding by initiating the aggregation of soluble α-Syn-FL with preformed α-Syn-CT119 fibrils. While a seeding effect was observed, the acceleration induced by homotypic seeding was greater than that promoted by heterotypic interactions.

Given our observation that ZPD-2 targets oligomers and/or other early assemblies, we speculated that the addition of preformed fibrils might override its inhibitory capability. To our surprise, this was not the case, and the presence of the molecule at the beginning of the reaction almost completely prevented aggregation in all seeded and unseeded reactions (Fig. 8A,C,E), resulting in reductions in Th-T fluorescence of 97.05%, 91.25% for α-Syn-FL and α-Syn-CT119 homotypic seeding, respectively, and 91.9% for the cross-seeded reaction. This anti-aggregational effect of ZPD-2 was further confirmed by light scattering measurements (Fig. 8B,D,F). SC-D also exhibited anti-seeding activity, albeit much lower than that of ZPD-2 in all cases, with efficacy varying depending on the identity of the soluble protein and the added seed (Fig. 8).

Discussion

The aggregation of α-Syn is considered to play a major role in the onset and progression of PD. Diverse truncated forms of α-Syn have been observed in neuronal deposits, corresponding to up to 20% of the total aggregated protein. Even though the exact role in the pathogenesis of these truncated variants remains unknown, truncations on the C-terminal region have been shown to markedly enhance the aggregation propensity of α-Syn. Accordingly, it has been suggested that the aggregation of C-terminally truncated forms precedes and promotes the aggregation of the full-length protein *in vivo*. In this scenario, targeting the aggregation of C-terminal truncated α-Syn emerges as an attractive therapeutic approach for PD treatment. Despite several molecules that have been described to prevent α-Syn aggregation, the modulation of C-terminally truncated α-Syn aggregation is still a poorly explored strategy, and to the best of our knowledge, only one small molecule has been described to display such activity [40].

In this study, we investigate the effect of inhibitors of α-Syn aggregation, SC-D and ZPD-2, on the polymerisation of the 1—119 truncated form. Th-T analysis (Fig. 4) demonstrated that both compounds can modulate the aggregation of α-Syn-CT119 *in vitro*, a finding corroborated by light-scattering and TEM (Fig. 4). These results suggest that the previously described inhibitory activity of these compounds on a-Syn-FL aggregation does not involve direct interaction with the C-terminal domain, unlike what has been observed with other molecules [55,56]. Titration assays (Fig. 5) revealed that ZPD-2 has a significantly higher *in vitro* inhibitory potential compared to SC-D, which did not show significant substoichiometric anti-aggregational capacity. Time-dependent assays (Fig. 6) indicated that ZPD-2's activity on α-Syn-CT119 largely depends on the stage of the aggregation process, with inhibitory effects being most potent when the molecule is present at the onset of the reaction. To note, this behaviour aligns with our previous hypothesis [57] and results for α-Syn-FL [41,42].

To confirm this view, we incubated α-Syn-CT119 oligomers in the presence or absence of the compounds. The lack of the C-terminal region promotes the lateral association of α-Syn-CT119 oligomers into chains, without significantly impacting the structure of the core compared to FL oligomers [36,48]. This provides an excellent tool to analyse the anti-oligomeric properties of a given compound. SC-D had a negligible effect, showing no significant impact on the number or morphology of these structures (Fig. 7). In contrast, ZPD-2 targeted the oligomers, disintegrating them, likely by altering their surface properties, resulting in a decreased number of oligomers upon treatment and the remaining aggregates appearing less spherical and more clustered, further supporting ZPD-2 acting on early intermediates in aggregation reactions (Fig. 7). This suggests that the strong ZPD-2 inhibitory capacity may be associated with off-pathway processes that generate non-productive assemblies, which could explain the lower effect of the molecule on the scattering signal compared to Th-T fluorescence (Fig. 4).

Surprisingly, homotypic and heterotypic seeding reactions revealed that both compounds were capable of acting on seeded processes (Fig. 8). ZPD-2, in particular, exhibited strong inhibitory potential in all

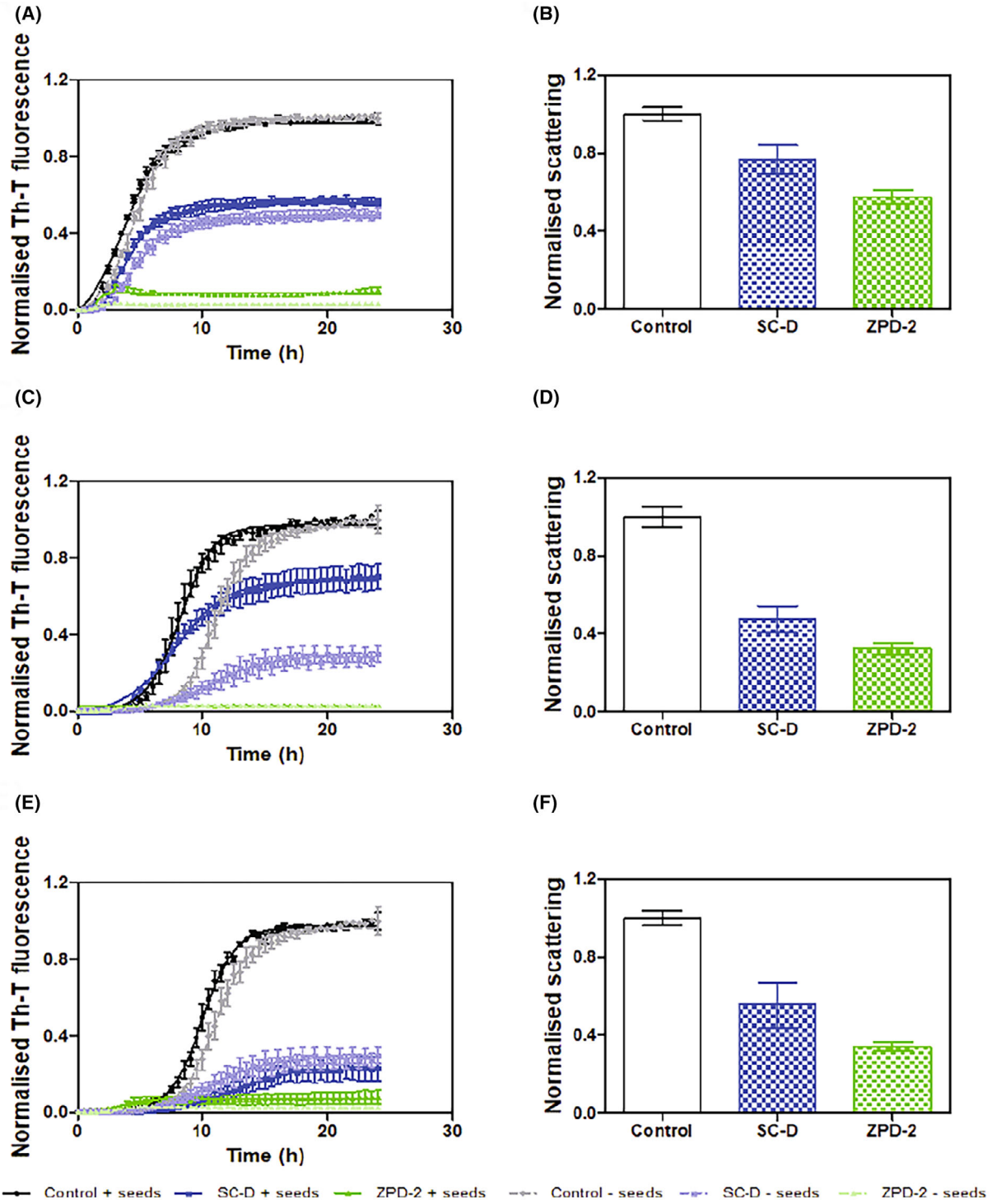

Fig. 8. Effect of the compounds on the seeded polymerisation. (A, B) Seeded aggregation of C-terminally truncated α-Syn reported by Th-T derived fluorescence (A) and light-scattering (B) at final point. (C, D) Seeded aggregation of *wt* α-Syn reported by Th-T derived fluorescence (C) and light-scattering (D) at final point. (E, F) Seeded aggregation of *wt* α-Syn by using seeds from C-terminally α-Syn fibrils reported by Th-T derived fluorescence (E) and light-scattering (F) at final point. In all cases the protein was incubated in absence (black) or in presence of 50 μM of SC-D (blue) and ZPD-2 (green); lighter colours in the kinetic reactions represent unseeded reactions. Th-T fluorescence and light scattering are plotted as normalised means. Error bars are shown as standard errors of mean values. All the experimental data, acquired in three independent experiments ($n = 3$).

seeded reactions. This strongly suggests that the molecule interferes with the fibril-catalysed secondary nucleation in the autocatalytic proliferation of α-Syn fibrils. Since in seeded reactions, oligomers are generated primarily by surface-catalysed secondary nucleation [58,59], the ability of ZPD-2 to interfere with these species might account for the observed activity. The ability of ZPD-2 to strongly inhibit both spontaneous and seeded polymerisation of α-Syn-CT119 underscores its potential as a therapeutic agent. This dual action suggests that ZPD-2 can not only prevent the initial aggregation of α-Syn but also impede the propagation of existing aggregates, which is crucial in addressing the pathology of PD.

Conclusion

All in all, the results described here show that ZPD-2 holds great potential as a modulator of the aggregation of α-Syn-CT119 by targeting the initial stages of the process. The existence and aggregation of these truncated species are thought to precede and promote the aggregation of α-Syn-FL *in vivo*. Thus, preventing their aggregation addresses a critical aspect of PD pathology. Moreover, this study underscores the need to explore the inhibitory potential of hit compounds beyond the traditional assays focused exclusively on full-length α-Syn, including the study of truncations and other post-transductional modifications.

Methods

Protein expression and purification

The expression and purification of *wt* (used as a reference in this work) and C-terminally truncated α-Syn was performed as previously described [60], with slight adaptations for the truncated form. Protein expression was performed in an *Escherichia coli* BL21 DE3 strain, incubated in LB medium supplemented with 100 μM ampicillin, at 37 °C and 250 ***g***. Induction was conducted by the addition of 1 mM IPTG for 5 h at OD_{600} 0.6–0.8. Then, the cells were harvested upon 15 min of centrifugation at 4000 ***g*** and washed by resuspension and centrifugation with PBS 1×. Cell pellets were stored at −80 °C until used. Once required, the pellet was resuspended in 50 mL of lysis buffer per 1 L of culture, composed of 50 mM Tris, 150 mM NaCl, 1 mM PMSF or 0.02 $mg{\cdot}mL^{-1}$ DNase, 1 mM EDTA, 1 mM benzamidine, 1 $\mu g{\cdot}mL^{-1}$ pepstatin, tip covered spoon of lysozyme, pH 7.4 for *wt* variant or pH 9.0 for truncated variant. The resuspended cells were sonicated with a LABSONICU sonicator (B. Braun Biotech International, Ventura, CA, USA) for 7.5 min at 35% amplitude, 2 s ON and 2 s OFF, and centrifuged for 30 min at 20 000 ***g***. The soluble fraction was then recovered and incubated for 15 min at 95 °C. Then, the sample was centrifuged for 30 min at 20 000 ***g*** and the soluble fraction treated with 4.7 g of streptomycin sulphate and incubated 15 min at 4 °C and mild shaking. Afterwards, the samples were centrifuged at 20 000 ***g*** for 15 min. The soluble fraction was then recovered and mixed with 360 $mg{\cdot}mL^{-1}$ of ammonium sulphate. After 20 min of incubation at 4 °C and mild shaking, the mixture was centrifuged at 20 000 ***g*** for 20 min and the pellet recovered. The pellet was finally resuspended on Tris/HCl 100 mM pH 9.0 (truncated variant) or pH 8.0 (*wt* variant) and dialysed (4–5 h and overnight) with Tris/HCl 25 mM pH 9.0 (truncated variant) or pH 8.0 (*wt* variant). After dialysis, the sample was filtered with a 0.22-μm filter and loaded into an anion exchange column HiTrap Q HP (GE Healthcare, Chicago, IL, USA) coupled to an ÄKTA purifier high-performance liquid chromatography system (GE Healthcare). Tris 25 mM pH 8.0 or 9.0 and Tris 25 mM pH 8.0 or 9.0 with NaCl 500 mM were used as buffer A and buffer B, respectively. The protein was eluted implementing a step gradient: step 1, 0% buffer B, 5 cv; step 2, 20% buffer B, 5 cv; step 3, 50% buffer B, 5 cv; step 4, 75% buffer B, 5 cv; step 5, 100% buffer B, 5 cv. The obtained protein was then loaded into a gel filtration chromatography with 50 mM ammonium acetate pH 8.0. To conclude, the protein was lyophilised for 48 h and stored at −80 °C until used.

Protein aggregation

To aggregate both *wt* and C-terminally truncated α-Syn, the lyophilised proteins were first resuspended on PBS 1× to a final concentration of 210 μM and filtered through a 0.22 μm filter to remove small aggregates and contaminants derived from resuspension. The aggregation was performed on a 96-well plate in which each well contains 35 μM of α-Syn, 40 μM Th-T, a 1/8″ diameter Teflon polyball (Polysciences Europe GmbH, Hirschberg an der Bergstraße, Germany) and 50 μM of the compounds. As a control reference, the same volume of DMSO (2.5%) was added. The final volume of the reaction was 150 μL. The plate was incubated at 37 °C with continuous orbital shaking (96 ***g***) in a SPARK® multimode microplate reader (Tecan, Männedorf, Switzerland). Th-T fluorescent increase was measured every hour by exciting at 445 nm and collecting fluorescence emission at 495 for 24 h.

In later kinetic studies, the concentration of α-Syn remained constant at 35 μM, while the compounds were added at different concentrations ranging from 50 to 5 μM. As reference, DMSO content was maintained identically in all the wells (2.5%). Also, the capacity of targeting the seeded polymerisation of the protein was analysed by adding 0.1% (v/v) of seeds to 35 μM of α-Syn, with or without 50 μM of the compounds. The seeds

were obtained from mature fibrils formed as previously, which were sonicated three times at 35%, 40s with 1ON–3OFF cycles. In further kinetics assays, the aggregation was performed at 35 μM in presence or absence of the compounds; however, the compounds or DMSO were added at different time-points (2.5 and 5 h) at a final concentration of 50 μM.

Each assay was done in triplicate and the values of the kinetic fitted according to the following equation:

$$\propto = 1 - \frac{1}{k_b(e^{k_a t - 1}) + 1}$$

where k_b and k_a constitute the homogeneous nucleation rate constant and the autocatalytic rate constant, respectively [61].

Oligomeric formation was performed as previously [46,49]. Briefly, purified α-Syn was previously dialysed against Milli-Q water and lyophilised for 48 h in aliquots of 6 mg. Lyophilised protein was resuspended in 500 μL of PBS 1× to a final concentration of 800 μM, filtered through 0.22 μm filters and incubated at 37 °C on quiescent conditions for 20–24 h. The resultant samples were ultracentrifuged at 288 000 ***g*** for 1 h in a SW55Ti Beckman rotor to remove any fibrillar structure formed during the incubation. Finally, the oligomers were filtered four times using 100 kDa centrifuge filters (Merck, Darmstadt, Germany) to remove the remaining monomeric protein. The resultant oligomers were diluted to a final concentration of 20 μM of protein and incubated in presence of 100 μM of the compounds (or DMSO) for 24 h at 25 °C in quiescent conditions.

Secondary structure determination

Attenuated total reflection Fourier-transform infrared (ATR-FTIR) spectroscopy analysis was performed using a Bruker Tensor 27 FTIR Spectrometer (Bruker Optics Inc, Billerica, MA, USA) with a Golden Gate MKII ATR accessory. All the spectra consist of 16 independent scans, measured at a spectral resolution of 4 cm^{-1}, within the 1800–1500 cm^{-1} range. Second derivatives of the spectra were used to determine the secondary composition. Fourier-deconvolution and determination of band position of the original amide I band were performed using PEAKFIT software (Grafiti LLC, Palo Alto, CA, USA).

Light-scattering measurements

To validate Th-T outcomes, 80 μL of the resultant aggregates were resuspended and recovered into a quartz cuvette. The scattering was then recorded in a Cary Eclipse Fluorescence Spectrophotometer (Agilent, Santa Clara, CA, USA) by exciting the samples at 340 nm and collecting at 330–350 nm. The sample of each well was measured independently, and technical triplicates were implemented.

Transmission electron microscopy (TEM)

Incubated fibrils at 70 μM in presence or absence of 200 μM of the different compounds were recovered and diluted 1:10 in PBS 1× and sonicated for 30 s, with an intensity level of 2 to reduce the number of large clusters. The grids were previously glow discharged for 25 s, at 25 mA and 0.37 mBar. Then, 5 μL of the samples were placed on the grid for 1 min and the excess removed with a filter paper. Afterwards, the grids were washed twice in milli-Q water, which was removed as before. Finally, 5 μL of a 2% (w/v) uranyl acetate solution were added to the grid as negative staining for 1 min and thus removed as previously. Representative TEM images were acquired with a Transmission Electron Microscopy Jeol 1400 (JEOL USA, Inc., Peabody, MA, USA), at an accelerating voltage of 120 kV. At least 30 fields per sample were screened.

Acknowledgements

We thank the Servei de Microscòpia at Universitat Autònoma de Barcelona for their help with TEM. SV was supported by the Spanish Ministry of Science and Innovation (PID2022-137963OB-I00), ICREA (ICREA-Academia 2020), AGAUR (Generalitat de Catalunya) (SGR2021-00635), CERCA Programme (Generalitat de Catalunya) and the Fundación La Marató de TV3 (Ref. 20144330). We thank Jordi Pujols for the design of the plasmid and Jaime Santos and Manuel Baño-Polo for designing the purification protocol.

Conflict of interest

The authors declare no conflict of interest.

Author contributions

SP-D and SV—conceptualisation; SP-D—methodology; SP-D and SV—formal analysis; SP-D—investigation; SP-D and SV—writing: original draft; SV—supervision; SV—project administration; SV—funding acquisition.

Peer review

The peer review history for this article is available at https://www.webofscience.com/api/gateway/wos/peer-review/10.1111/febs.17310.

Data availability statement

The data that support the findings of this study are available from the corresponding author upon reasonable request.

References

1 Dexter DT & Jenner P (2013) Parkinson disease: from pathology to molecular disease mechanisms. *Free Radic Biol Med* **62**, 132–144.
2 Kalia LV & Lang AE (2015) Parkinson's disease. *Lancet* **386**, 896–912.
3 Tolosa E, Wenning G & Poewe W (2006) The diagnosis of Parkinson's disease. *Lancet Neurol* **5**, 75–86.
4 Marti MJ, Tolosa E & Campdelacreu J (2003) Clinical overview of the synucleinopathies. *Mov Disord* **18**(Suppl 6), S21–S27.
5 Duncan GW, Khoo TK, Yarnall AJ, O'Brien JT, Coleman SY, Brooks DJ, Barker RA & Burn DJ (2014) Health-related quality of life in early Parkinson's disease: the impact of nonmotor symptoms. *Mov Disord* **29**, 195–202.
6 Martinez-Martin P, Rodriguez-Blazquez C, Kurtis MM, Chaudhuri KR & NMSS Validation Group (2011) The impact of non-motor symptoms on health-related quality of life of patients with Parkinson's disease. *Mov Disord* **26**, 399–406.
7 Spillantini MG, Schmidt ML, Lee VM, Trojanowski JQ, Jakes R & Goedert M (1997) Alpha-synuclein in Lewy bodies. *Nature* **388**, 839–840.
8 Bendor JT, Logan TP & Edwards RH (2013) The function of alpha-synuclein. *Neuron* **79**, 1044–1066.
9 Sun J, Wang L, Bao H, Premi S, Das U, Chapman ER & Roy S (2019) Functional cooperation of alpha-synuclein and VAMP2 in synaptic vesicle recycling. *Proc Natl Acad Sci USA* **116**, 11113–11115.
10 Burre J, Sharma M, Tsetsenis T, Buchman V, Etherton MR & Sudhof TC (2010) Alpha-synuclein promotes SNARE-complex assembly in vivo and in vitro. *Science* **329**, 1663–1667.
11 Burre J, Sharma M & Sudhof TC (2014) Alpha-synuclein assembles into higher-order multimers upon membrane binding to promote SNARE complex formation. *Proc Natl Acad Sci USA* **111**, E4274–E4283.
12 Hallacli E, Kayatekin C, Nazeen S, Wang XH, Sheinkopf Z, Sathyakumar S, Sarkar S, Jiang X, Dong X, Di Maio R *et al*. (2022) The Parkinson's disease protein alpha-synuclein is a modulator of processing bodies and mRNA stability. *Cell* **185**, e33.
13 Schaser AJ, Osterberg VR, Dent SE, Stackhouse TL, Wakeham CM, Boutros SW, Weston LJ, Owen N, Weissman TA, Luna E *et al*. (2019) Alpha-synuclein is a DNA binding protein that modulates DNA repair with implications for Lewy body disorders. *Sci Rep* **9**, 10919.
14 Serpell LC, Berriman J, Jakes R, Goedert M & Crowther RA (2000) Fiber diffraction of synthetic alpha-synuclein filaments shows amyloid-like cross-beta conformation. *Proc Natl Acad Sci USA* **97**, 4897–4902.
15 Fusco G, De Simone A, Gopinath T, Vostrikov V, Vendruscolo M, Dobson CM & Veglia G (2014) Direct observation of the three regions in alpha-synuclein that determine its membrane-bound behaviour. *Nat Commun* **5**, 3827.
16 Rodriguez JA, Ivanova MI, Sawaya MR, Cascio D, Reyes FE, Shi D, Sangwan S, Guenther EL, Johnson LM, Zhang M *et al*. (2015) Structure of the toxic core of alpha-synuclein from invisible crystals. *Nature* **525**, 486–490.
17 Guerrero-Ferreira R, Taylor NM, Mona D, Ringler P, Lauer ME, Riek R, Britschgi M & Stahlberg H (2018) Cryo-EM structure of alpha-synuclein fibrils. *elife* **7**, e36402.
18 Chakraborty R & Chattopadhyay K (2019) Cryo-electron microscopy uncovers key residues within the core of alpha-synuclein fibrils. *ACS Chem Neurosci* **10**, 1135–1136.
19 Jao CC, Hegde BG, Chen J, Haworth IS & Langen R (2008) Structure of membrane-bound alpha-synuclein from site-directed spin labeling and computational refinement. *Proc Natl Acad Sci USA* **105**, 19666–19671.
20 Ulmer TS, Bax A, Cole NB & Nussbaum RL (2005) Structure and dynamics of micelle-bound human alpha-synuclein. *J Biol Chem* **280**, 9595–9603.
21 Hoyer W, Cherny D, Subramaniam V & Jovin TM (2004) Impact of the acidic C-terminal region comprising amino acids 109-140 on alpha-synuclein aggregation in vitro. *Biochemistry* **43**, 16233–16242.
22 Izawa Y, Tateno H, Kameda H, Hirakawa K, Hato K, Yagi H, Hongo K, Mizobata T & Kawata Y (2012) Role of C-terminal negative charges and tyrosine residues in fibril formation of alpha-synuclein. *Brain Behav* **2**, 595–605.
23 Santos J, Iglesias V, Santos-Suarez J, Mangiagalli M, Brocca S, Pallares I & Ventura S (2020) pH-dependent aggregation in intrinsically disordered proteins is determined by charge and lipophilicity. *Cells* **9**, 145.
24 Li W, West N, Colla E, Pletnikova O, Troncoso JC, Marsh L, Dawson TM, Jakala P, Hartmann T, Price DL *et al*. (2005) Aggregation promoting C-terminal truncation of alpha-synuclein is a normal cellular process and is enhanced by the familial Parkinson's disease-linked mutations. *Proc Natl Acad Sci USA* **102**, 2162–2167.
25 Murray IV, Giasson BI, Quinn SM, Koppaka V, Axelsen PH, Ischiropoulos H, Trojanowski JQ & Lee VM (2003) Role of alpha-synuclein carboxy-terminus on fibril formation in vitro. *Biochemistry* **42**, 8530–8540.
26 Ma L, Yang C, Zhang X, Li Y, Wang S, Zheng L & Huang K (2018) C-terminal truncation exacerbates the aggregation and cytotoxicity of alpha-synuclein: a vicious cycle in Parkinson's disease. *Biochim Biophys Acta Mol basis Dis* **1864**, 3714–3725.

27 Sorrentino ZA & Giasson BI (2020) The emerging role of alpha-synuclein truncation in aggregation and disease. *J Biol Chem* **295**, 10224–10244.
28 Liu CW, Giasson BI, Lewis KA, Lee VM, Demartino GN & Thomas PJ (2005) A precipitating role for truncated alpha-synuclein and the proteasome in alpha-synuclein aggregation: implications for pathogenesis of Parkinson disease. *J Biol Chem* **280**, 22670–22678.
29 Mishizen-Eberz AJ, Guttmann RP, Giasson BI, Day GA 3rd, Hodara R, Ischiropoulos H, Lee VM, Trojanowski JQ & Lynch DR (2003) Distinct cleavage patterns of normal and pathologic forms of alpha-synuclein by calpain I in vitro. *J Neurochem* **86**, 836–847.
30 Mahul-Mellier AL, Burtscher J, Maharjan N, Weerens L, Croisier M, Kuttler F, Leleu M, Knott GW & Lashuel HA (2020) The process of Lewy body formation, rather than simply alpha-synuclein fibrillization, is one of the major drivers of neurodegeneration. *Proc Natl Acad Sci USA* **117**, 4971–4982.
31 Games D, Valera E, Spencer B, Rockenstein E, Mante M, Adame A, Patrick C, Ubhi K, Nuber S, Sacayon P *et al*. (2014) Reducing C-terminal-truncated alpha-synuclein by immunotherapy attenuates neurodegeneration and propagation in Parkinson's disease-like models. *J Neurosci* **34**, 9441–9454.
32 Stephens AD, Zacharopoulou M, Moons R, Fusco G, Seetaloo N, Chiki A, Woodhams PJ, Mela I, Lashuel HA, Phillips JJ *et al*. (2020) Extent of N-terminus exposure of monomeric alpha-synuclein determines its aggregation propensity. *Nat Commun* **11**, 2820.
33 Zhang C, Pei Y, Zhang Z, Xu L, Liu X, Jiang L, Pielak GJ, Zhou X, Liu M & Li C (2022) C-terminal truncation modulates alpha-Synuclein's cytotoxicity and aggregation by promoting the interactions with membrane and chaperone. *Commun Biol* **5**, 798.
34 Sorrentino ZA, Xia Y, Gorion KM, Hass E & Giasson BI (2020) Carboxy-terminal truncations of mouse alpha-synuclein alter aggregation and prion-like seeding. *FEBS Lett* **594**, 1271–1283.
35 Terada M, Suzuki G, Nonaka T, Kametani F, Tamaoka A & Hasegawa M (2018) The effect of truncation on prion-like properties of alpha-synuclein. *J Biol Chem* **293**, 13910–13920.
36 Farzadfard A, Pedersen JN, Meisl G, Somavarapu AK, Alam P, Goksoyr L, Nielsen MA, Sander AF, Knowles TPJ, Pedersen JS *et al*. (2022) The C-terminal tail of alpha-synuclein protects against aggregate replication but is critical for oligomerization. *Commun Biol* **5**, 123.
37 Pena DS & Ventura S (2022) One ring is sufficient to inhibit alpha-synuclein aggregation. *Neural Regen Res* **17**, 508–511.
38 Pena-Diaz S, Garcia-Pardo J & Ventura S (2023) Development of small molecules targeting alpha-synuclein aggregation: a promising strategy to treat Parkinson's disease. *Pharmaceutics* **15**, 839.
39 Pujols J, Pena-Diaz S, Pallares I & Ventura S (2020) Chemical chaperones as novel drugs for Parkinson's disease. *Trends Mol Med* **26**, 408–421.
40 Kim J, Harada R, Kobayashi M, Kobayashi N & Sode K (2010) The inhibitory effect of pyrroloquinoline quinone on the amyloid formation and cytotoxicity of truncated alpha-synuclein. *Mol Neurodegener* **5**, 20.
41 Pena-Diaz S, Pujols J, Conde-Gimenez M, Carija A, Dalfo E, Garcia J, Navarro S, Pinheiro F, Santos J, Salvatella X *et al*. (2019) ZPD-2, a small compound that inhibits alpha-synuclein amyloid aggregation and its seeded polymerization. *Front Mol Neurosci* **12**, 306.
42 Pujols J, Pena-Diaz S, Lazaro DF, Peccati F, Pinheiro F, Gonzalez D, Carija A, Navarro S, Conde-Gimenez M, Garcia J *et al*. (2018) Small molecule inhibits alpha-synuclein aggregation, disrupts amyloid fibrils, and prevents degeneration of dopaminergic neurons. *Proc Natl Acad Sci USA* **115**, 10481–10486.
43 van der Wateren IM, Knowles TPJ, Buell AK, Dobson CM & Galvagnion C (2018) C-terminal truncation of alpha-synuclein promotes amyloid fibril amplification at physiological pH. *Chem Sci* **9**, 5506–5516.
44 Tuttle MD, Comellas G, Nieuwkoop AJ, Covell DJ, Berthold DA, Kloepper KD, Courtney JM, Kim JK, Barclay AM, Kendall A *et al*. (2016) Solid-state NMR structure of a pathogenic fibril of full-length human alpha-synuclein. *Nat Struct Mol Biol* **23**, 409–415.
45 Li B, Ge P, Murray KA, Sheth P, Zhang M, Nair G, Sawaya MR, Shin WS, Boyer DR, Ye S *et al*. (2018) Cryo-EM of full-length alpha-synuclein reveals fibril polymorphs with a common structural kernel. *Nat Commun* **9**, 3609.
46 Santos J, Cuellar J, Pallares I, Byrd EJ, Lends A, Moro F, Abdul-Shukkoor MB, Pujols J, Velasco-Carneros L, Sobott F *et al*. (2024) A targetable N-terminal motif orchestrates alpha-synuclein oligomer-to-fibril conversion. *J Am Chem Soc* **146**, 12702–12711.
47 Pena-Diaz S, Pujols J, Vasili E, Pinheiro F, Santos J, Manglano-Artunedo Z, Outeiro TF & Ventura S (2022) The small aromatic compound SynuClean-D inhibits the aggregation and seeded polymerization of multiple alpha-synuclein strains. *J Biol Chem* **298**, 101902.
48 Franco A, Cuellar J, Fernandez-Higuero JA, de la Arada I, Orozco N, Valpuesta JM, Prado A & Muga A (2021) Truncation-driven lateral association of alpha-synuclein hinders amyloid clearance by the Hsp70-based Disaggregase. *Int J Mol Sci* **22**, 12983.
49 Santos J, Gracia P, Navarro S, Pena-Diaz S, Pujols J, Cremades N, Pallares I & Ventura S (2021) Alpha-helical peptidic scaffolds to target alpha-synuclein toxic species with nanomolar affinity. *Nat Commun* **12**, 3752.
50 Tornquist M, Michaels TCT, Sanagavarapu K, Yang X, Meisl G, Cohen SIA, Knowles TPJ & Linse S (2018) Secondary nucleation in amyloid formation. *Chem Commun (Camb)* **54**, 8667–8684.

51 Luk KC, Kehm V, Carroll J, Zhang B, O'Brien P, Trojanowski JQ & Lee VM (2012) Pathological alpha-synuclein transmission initiates Parkinson-like neurodegeneration in nontransgenic mice. *Science* **338**, 949–953.
52 Luk KC, Kehm VM, Zhang B, O'Brien P, Trojanowski JQ & Lee VM (2012) Intracerebral inoculation of pathological alpha-synuclein initiates a rapidly progressive neurodegenerative alpha-synucleinopathy in mice. *J Exp Med* **209**, 975–986.
53 Masuda-Suzukake M, Nonaka T, Hosokawa M, Oikawa T, Arai T, Akiyama H, Mann DM & Hasegawa M (2013) Prion-like spreading of pathological alpha-synuclein in brain. *Brain* **136**, 1128–1138.
54 Gribaudo S, Tixador P, Bousset L, Fenyi A, Lino P, Melki R, Peyrin JM & Perrier AL (2019) Propagation of alpha-synuclein strains within human reconstructed neuronal network. *Stem Cell Rep* **12**, 230–244.
55 Mazzulli JR, Armakola M, Dumoulin M, Parastatidis I & Ischiropoulos H (2007) Cellular oligomerization of alpha-synuclein is determined by the interaction of oxidized catechols with a C-terminal sequence. *J Biol Chem* **282**, 31621–31630.
56 Herrera FE, Chesi A, Paleologou KE, Schmid A, Munoz A, Vendruscolo M, Gustincich S, Lashuel HA & Carloni P (2008) Inhibition of alpha-synuclein fibrillization by dopamine is mediated by interactions with five C-terminal residues and with E83 in the NAC region. *PLoS One* **3**, e3394.
57 Pena-Diaz S, Pujols J & Ventura S (2020) Small molecules to prevent the neurodegeneration caused by alpha-synuclein aggregation. *Neural Regen Res* **15**, 2260–2261.
58 Michaels TC, Lazell HW, Arosio P & Knowles TP (2015) Dynamics of protein aggregation and oligomer formation governed by secondary nucleation. *J Chem Phys* **143**, 054901.
59 Gaspar R, Meisl G, Buell AK, Young L, Kaminski CF, Knowles TPJ, Sparr E & Linse S (2017) Secondary nucleation of monomers on fibril surface dominates alpha-synuclein aggregation and provides autocatalytic amyloid amplification. *Q Rev Biophys* **50**, e6.
60 Pujols J, Pena-Diaz S, Conde-Gimenez M, Pinheiro F, Navarro S, Sancho J & Ventura S (2017) High-throughput screening methodology to identify alpha-synuclein aggregation inhibitors. *Int J Mol Sci* **18**, 478.
61 Crespo R, Villar-Alvarez E, Taboada P, Rocha FA, Damas AM & Martins PM (2016) What can the kinetics of amyloid fibril formation tell about off-pathway aggregation? *J Biol Chem* **291**, 2018–2032.